

Dimensionality of mobile electrons at X-ray-irradiated LaAlO₃/SrTiO₃ interfaces

V. N. Strocov,¹ F. Lechermann,² A. Chikina,¹ F. Alarab,¹ L. L. Lev,^{1,3} V. A. Rogalev,^{1,4} T. Schmitt,¹ and M.-A. Husanu^{1,5}

¹Swiss Light Source, Paul Scherrer Institute, CH-5232 Villigen-PSI, Switzerland

²Institut für Theoretische Physik, Universität Hamburg, Jungiusstr. 9, DE-20355 Hamburg, Germany

³Moscow Institute of Physics and Technology, 9 Institutskiy lane, RU-141700 Dolgoprudny, Russia

⁴Julius-Maximilians-Universität, Physikalisches Institut, Am Hubland, 97074 Würzburg, Germany

⁵National Institute of Materials Physics, Atomistilor 405A, RO-077125 Magurele, Romania

Electronic structure of LaAlO₃/SrTiO₃ (LAO/STO) samples, grown at low oxygen pressure and post-annealed ex-situ, was investigated by soft-X-ray ARPES focussing on the Fermi momentum (\mathbf{k}_F) of the mobile electron system (MES). X-ray irradiation of these samples at temperatures below 100K creates oxygen vacancies (V_{O_s}) injecting Ti t_{2g} -electrons into the MES. At this temperature the oxygen out-diffusion is suppressed, and the V_{O_s} should appear mostly in the top STO layer. The X-ray generated MES demonstrates, however, a pronounced three-dimensional (3D) behavior as evidenced by variations of its experimental \mathbf{k}_F over different Brillouin zones. Identical to bare STO, this behavior indicates an unexpectedly large extension of the X-ray generated MES into the STO depth. The intrinsic MES in the standard LAO/STO samples annealed in-situ, in contrast, demonstrates purely two-dimensional (2D) behaviour. Based on self-interaction-corrected DFT calculations of the MES induced by V_{O_s} at the interface and in STO bulk, we discuss possible scenarios of the puzzling 3D-ity. It may involve either a dense ladder of quantum-well states formed in a long-range interfacial potential or, more likely, X-ray-induced bulk metallicity in STO accessed in the ARPES experiment through a short-range interfacial barrier. The mechanism of this metallicity may involve remnant V_{O_s} and photoconductivity-induced metallic states in the STO bulk, and even more exotic mechanisms such as X-ray induced formation of Frenkel pairs.

Introduction

Transition-metal oxides (TMOs) presently play one of the forefront roles in theoretical and experimental condensed matter research (for entries see [1]). An involved interplay between the spin, charge, orbital and lattice degrees of freedom in these materials results in a wealth of phenomena interesting from the fundamental point of view and bearing potential for technological applications. These include rich electronic and magnetic phase diagrams, metal-insulator transitions, colossal magnetoresistance, ferroelectricity, multiferroicity, high- T_c superconductivity, etc. Interfaces and heterostructures of TMOs can add another dimension to their fascinating properties, giving rise to physical phenomena which cannot be anticipated from the properties of individual constituents, with the new functionalities having great promise for future device applications (see, for example, the reviews [2,3]).

The interface between LaAlO_3 (LAO) and SrTiO_3 (STO) is a paradigm example of new functionalities that can be formed by interfacing TMOs. Although bulk LAO and STO are both band insulators, their interface spontaneously forms a mobile electron system (MES) [2,3]. Its high electron mobility co-exists with superconductivity, ferromagnetism, large magnetoresistance and other non-trivial phenomena which can in addition be tuned with field effect. The MES electrons are localized in the interfacial quantum well (QW) on the STO side and populate the Ti t_{2g} -derived in-plane d_{xy} -states and out-of-plane $d_{xz/yz}$ -states [4–6]. The latter, furthermore, can be manipulated through artificial quantum confinement in thin STO layers [7]. Whereas in stoichiometric LAO/STO the MES is localized within a few layers from the interface and is therefore purely 2D, oxygen deficiency of STO can extend the MES to a much larger depth of more than 1000 Å, resulting in its essentially 3D character [8–10]. Two phenomena bearing key importance for virtually all physical properties of LAO/STO are (1) polaronic nature of the charge carriers, where strong electron-phonon coupling to the LO3 phonon mode reduces their low-temperature mobility by a factor of about 2.5, and coupling to soft phonon modes dramatically reduces mobility with temperature [11,12], and (2) electronic phase separation (EPS) where the conducting MES puddles are embedded in the insulating host phase [12–14].

X-ray irradiation can dramatically change electronic and magnetic properties of oxide materials, which is typically connected with creation of oxygen vacancies (V_{O^s}) [14–22]. In a simplified picture of oxygen-deficient (OD) STO, each V_{O^s} releases two electrons from the neighbouring Ti atom. One of them joins the MES formed by delocalized quasiparticles, which are Ti t_{2g} derived, weakly correlated, non-magnetic and form large polarons [11]. The other electron stays near the Ti ion to form localized in-gap state (IGSs) at binding energy $E_b \sim -1.3$ eV, which are Ti e_g derived, strongly correlated, magnetic and are often viewed as small polarons. In a more elaborate picture, the electron distribution between the MES and IGSs depends on particular configurations of V_{O^s} [23] which tend to cluster [14]. The V_{O^s} have a dramatic effect on the transport properties of STO, with their concentration of only 0.03% transforming STO into metal [24]. This picture of dichotomic electron system in the bulk as well at the surfaces and interfaces of OD-STO can be described within the combination of density functional theory with explicit electron-correlation schemes, such as e.g. dynamical mean-field theory (DMFT) (see, for example, Refs. [21,25–29]). Recently, it has been experimentally confirmed by resonant photoemission (ResPE) [22]. The coexistence of the two radically different MES and IGS electron subsystems hugely enriches the physics of

the OD-STO systems compared to the stoichiometric ones, critically affecting the conductivity, magnetism and EPS.

Here, we use soft-X-ray angle-resolved photoelectron spectroscopy (ARPES) to explore the dimensionality of the MES generated by X-ray irradiation of LAO/STO heterostructures grown in oxygen-deficient conditions and post-annealed (PA-LAO/STO). Our analysis focuses on variations of the experimental k_f across the Brillouin zones (BZs), with the k_f values determined from the gradient of bandwidth-integrated spectral intensity. Although the V_{0s} generated by X-rays at our low temperature of 12K should be located in the top STO layer, we observe an unexpected 3D-ity of X-ray generated MES, indicating its large extension into the STO depth. This behaviour, identical to the X-ray irradiated bare STO, contrasts with the 2D behavior of the intrinsic MES in standard LAO/STO samples. Based on self-interaction-corrected DFT calculations, we discuss possible scenarios how the 3D-MES is formed.

Sample preparation

Our LAO/STO samples with a LAO layer of the critical thickness 4 u.c. on top of TiO_2 -terminated STO(100) were grown with Pulsed Laser Deposition. We followed a non-standard growth protocol, where the STO substrate was annealed at 500°C in vacuum, the O_2 pressure during the LAO deposition at 720°C reduced to 8×10^{-5} mbar, and the post-growth annealing for 12 hrs performed ex-situ at a temperature of 500°C [14,22]. Although such samples are finally (nearly) stoichiometric in terms of the chemical-element ratio, as evidenced by their photoelectron spectroscopy characterization discussed below, their transport properties [30] are quite different from the LAO/STO samples grown and annealed under the standard protocol [11]. Their difference most important in the context of our ARPES study is that under X-ray irradiation at temperatures below $\sim 100K$ the post-annealed samples readily built up V_{0s} in STO. In the ARPES spectra acquired in parallel with the irradiation, this fact is evidenced by gradual development of the initially absent IGS peak in the band gap and Ti^{3+} component of the Ti $2p$ core levels, which are characteristic signatures of the V_{0s} (for detailed analysis of the time evolution see [14]).

The exact mechanism of irradiation-induced creation of V_{0s} at the LAO/STO interfaces and even bare STO surfaces is not yet quite understood. There are a few intriguing observations: (1) As unfolded below in this paper, the X-ray generated MES is 3D, suggesting its expansion over a significant depth into STO; (2) The X-ray generated V_{0s} and corresponding MES can be observed only at low sample temperatures below $\sim 100K$. Once created, they stay stable without further irradiation for at least tens of hours. Upon increase of temperature well above $\sim 100K$, however, they quench and can not develop even at relatively high synchrotron-radiation power densities (see below). This fact excludes that the classical thermally-activated diffusion of oxygen atoms out of STO be involved in the generation of the V_{0s} , because in this case the temperature dependence would be opposite. Instead, their creation and/or stabilization may in some way be linked to the cubic to tetragonal phase transition and concomitant creation of domains in STO below 105 K [31,32]. The electric field in STO due to the interfacial band bending, separating the photoexcited electrons and holes [33] as well as the repulsion of the mobile photoexcited electrons from the localized ones staying at the V_{0s} [34] may also contribute to the stability of the X-ray generated V_{0s} and MES; (3) The V_{0s} can be quenched by exposure of the LAO/STO samples to X-ray irradiation in O_2 pressure of about 10^{-7} mbar on a time scale of seconds, which is much faster than the generation of V_{0s} on a time scale of tens of

minutes. The high efficiency of this reaction can be explained by that X-ray irradiation cracks the physisorbed O_2 molecules into atomic oxygen [19,20]. We note that whereas for STO surfaces only absorption of O_2 molecules is sufficient to quench the V_{Os} [17], in our case of the buried LAO/STO interface their X-ray cracking is necessary. This observation can be explained, tentatively, by that oxygen would effectively penetrate through the LAO layer only in its atomic form; (4) The V_O -generation rate strongly depends on the sample growth protocol, including temperature and O_2 pressure during the substrate annealing and the LAO deposition, and in-situ vs ex-situ annealing. The LAO/STO samples grown under the standard protocol (ST-LAO/STO), including substrate annealing in O_2 , high O_2 pressure during the LAO deposition and in-situ annealing, are fairly immune to X-ray irradiation [11]. The susceptibility of the post-annealed samples to X-ray irradiation may be connected with certain amount of structural defects remaining in them after the post-annealing despite their complete or nearly complete stoichiometric recovery. At the moment, it is difficult to reconcile all these observations in one single mechanism of creation and stabilization of the V_{Os} , and this is not a prime objective of this study.

Experimental and theoretical methods

Our SX-ARPES experiments used ResPE at the Ti L -edge in order to boost the signal from the Ti derived electron states at the buried LAO/STO interface. The measurements were performed at the soft-X-ray ARPES endstation [35] of the Advanced Resonant Spectroscopies (ADRESS) beamline [36] at the Swiss Light Source, Paul Scherrer Institute, Switzerland. A photon flux of about 10^{13} photons/sec was focused in a spot size of $30 \times 75 \mu\text{m}^2$ on the sample surface, and the combined (beamline and analyzer) energy resolution (ΔE) was ~ 50 meV full width at half maximum (FWHM). The sample was kept at 12 K in order to suppress smearing of the k -dispersive spectral fraction [37] and, most importantly, allow a build-up of the V_{Os} under X-ray irradiation (see above). The X-ray absorption spectroscopy (XAS) data were measured in the total electron yield (TEY). All ARPES and XAS data presented below are acquired at saturation after more than 2 hrs of irradiation time. The XAS and angle-integrated photoemission data were measured with circularly polarized incident X-rays. The in-plane Fermi surface (FS) maps and ARPES band dispersion images presented below were measured with s -polarized X-rays, and the out-of-plane FS map with p -polarized X-rays.

Our electronic structure calculations for oxygen-deficient (OD) LAO/STO interfaces addressed possible MES contributions from V_{Os} in the top TiO_2 layer as well as in deeper-lying TiO_2 layers on equal footing as embedded in a LAO/STO supercell. The calculations utilized the STO-bulk lattice constant of $a=3.905 \text{ \AA}$, and were structurally relaxed within the generalized-gradient approximation (GGA) of Kohn-Sham's Density-Functional Theory (DFT) utilizing a mixed-basis pseudopotential code. The final electronic structure was determined with a DFT+self-interaction-correction (SIC) scheme, where explicit Coulomb interactions on oxygen sites are described within SIC, and are incorporated in the O pseudopotential [38]. The SIC was applied to the $O(2s)$ and the $O(2p)$ orbitals via weight factors w_p (see Ref. [38] for more details). While the $O(2s)$ orbital is by default fully corrected with $w_p=1.0$, the common choice $w_p=0.8$ was used for $O(2p)$ orbitals. Since the Ti t_{2g} states, mostly relevant for the MES, are only weakly occupied in LAO/STO, neglecting the explicit Coulomb interactions on Ti when focussing on the MES proves as an adequate approximation for the very large supercells. Note that when applied to bulk STO, the present DFT+SIC

treatment results in a reasonable band gap of 3 eV, curing the notorious underestimation in standard exchange-correlation functionals.

Electronic structure overview

Fig. 1 (a) shows the Ti $2p_{3/2}$ core-level spectrum of our PA-LAO/STO samples taken at $h\nu = 1000$ eV, which is decomposed into the Ti^{4+} and Ti^{3+} components (linear background removed). The latter is characteristic of the $V_{\text{O}s}$. (b) shows XAS spectrum through the Ti L_3 - and L_2 -edges (excited from the $2p_{3/2}$ and $2p_{1/2}$ core levels, respectively). The pairs of salient XAS peaks at each edge are formed by the $\text{Ti}^{4+} e_g$ and t_{2g} states. The corresponding map of ResPE intensity as a function of E_B and excitation energy $h\nu$, identifying the Ti-derived electron states [39–43] is displayed in Fig. 1 (c). Above the broad valence band composed from the O $2p$ states in STO and LAO, the map shows the resonating broad IGS peak at $E_B \sim -1.3$ eV which is a hallmark of the $V_{\text{O}s}$. Recent analysis of its resonant behavior [22] confirms that the IGS-subsystem is derived from e_g states of the Ti^{3+} ions pushed down in energy by strong electron correlations [25,27,28]. The narrow resonating peak at the Fermi energy (E_F) identifies the t_{2g} -derived MES. Its intensity maximum is shifted from the $\text{Ti}^{4+} t_{2g}$ to $\text{Ti}^{4+} e_g$ peak in the XAS spectrum due to remnant \mathbf{k} -conservation between the intermediate and final states coupled in the ResPE process [22].

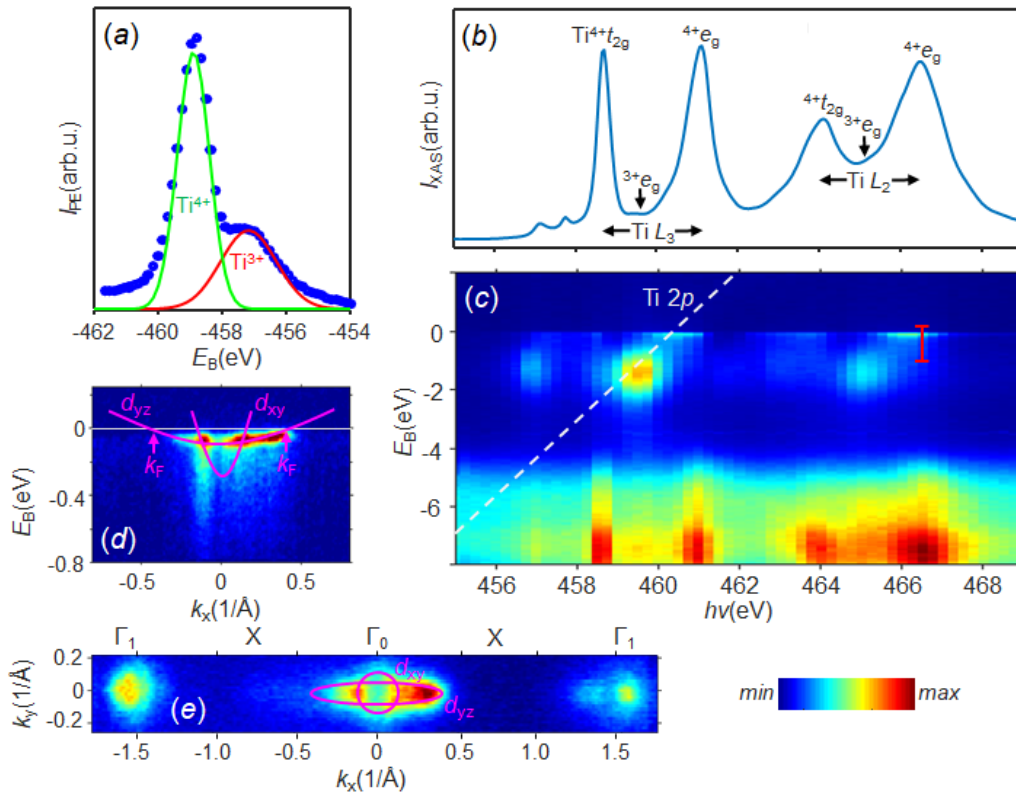


Fig. 1. Spectroscopic overview of PA-LAO/STO: (a) Ti $2p_{3/2}$ core level decomposed into the Ti^{4+} and Ti^{3+} components; (b) XAS spectrum and (c) angle-integrated ResPE intensity through the L_3 and L_2 edges. The resonating peak at E_F signals the t_{2g} -derived MES and the one at $E_B \sim -1.3$ eV the IGS characteristic of the $V_{\text{O}s}$; (d) the ARPES image along the ΓX direction measured at $h\nu = 466.4$ eV as marked by red bar at (c); (e) FS measured at the same $h\nu$. The d_{xy} and d_{yz} states, selected by the s-polarized X-rays, are indicated.

We note that $Ti^{3+} e_g$ and t_{2g} signals in the XAS spectrum in Fig. 1 (b), corresponding to the Ti atoms hosting the V_{O_s} , are almost invisible. At the same time, the IGS signal in the ResPE map (c), corresponding to the $Ti^{3+} e_g$ states of these atoms, is profound. This observation shows that most V_{O_s} are located in vicinity of the top STO layer, because the width of this region is much smaller than the probing depth of the TEY-XAS measurements of the order of 50 Å, and comparable with that of SX-ARPES measurements of the order of 11 Å at our excitation energy [20].

The image (d) in Fig. 1 shows the ARPES intensity measured along the ΓX direction with s -polarized incident X-rays, selecting predominantly the antisymmetric d_{xy} - and d_{yz} -derived electron states [6,11,22]. Furthermore, the choice of $h\nu = 466.4$ eV at the L_2 edge enhanced the d_{yz} states in comparison with the d_{xy} ones [22]. The ARPES data is overlaid with a sketch of the d_{xy} and d_{yz} dispersions. We note pronounced spectral intensity variations along the bands, caused by energy- and k -dependent photoemission matrix elements. Particularly remarkable is the spectral intensity asymmetry relative to the Γ points, absent in VUV-ARPES on bare STO surfaces [18,44]. With s -polarized X-rays in our experimental geometry, this phenomenon is beyond the conventional dipole approximation for the photoemission process (because the angle between the photoemission direction and electric vector of the light is the same) and should be attributed to the photon momentum that is $\sim 0.24 \text{ \AA}^{-1}$ for our $h\nu$ in the soft-X-ray energy range. We observe that for PA-LAO/STO the lowest d_{xy} band is much smeared compared to STO, and manifests itself as intensity hot spots where it intersects the d_{yz} band and hybridizes with it because of the symmetry breaking caused by the tetragonal lattice distortion and spin-orbit coupling. In view of the location of these d_{xy} states in the top TiO_2 layer, the observed smearing should be connected with a disorder induced in this layer by the LAO overlayer and X-ray generated V_{O_s} . As we will see below, the absence of high-order d_{xy} bands in PA-LAO/STO is consistent with the steeper electrostatic band-bending potential $V(z)$ compared to bare STO caused by the additional electron density injected by the V_{O_s} . We note that the band order and band dispersions observed in PA-LAO/STO (and STO) and ST-LAO/STO samples [6,11] demonstrate the same $d_{xy} < d_{xz/yz}$ band order. However, the observed band filling in PA-LAO/STO (STO) is somewhat larger than in ST-LAO/STO. Furthermore, the polaronic-hump weight and thus renormalization of the effective mass m^* in PA-LAO/STO (STO) reduce to ~ 1.5 compared to ~ 2.5 in ST-LAO/STO [11]. Importantly, as we will see below, these materials demonstrate different dimensionality of the MES. Finally, Fig. 1 (e) shows the experimental FS of PA-LAO/STO where we observe the circular d_{xy} and elliptical d_{yz} sheets.

Dimensionality of the MES

Do the MES electrons in PA-LAO/STO, developing under irradiation, stay confined at the interface and keep their 2D character, or expand into the STO bulk and become 3D? To answer this question, we investigated their ARPES response as a function of out-of-plane momentum k_z varied in an extended $h\nu$ -range above the Ti L -edge. Because of the much weaker off-resonance response of the MES, such measurements are extremely photon hungry. We used p -polarization of incident X-rays to switch from the two-band combination of the d_{xy} and d_{yz} antisymmetric states to the single-band d_{xz} state. Fig. 2 shows an experimental map of ARPES intensity at E_F as a function of $h\nu$, rendered into the out-of-plane momentum k_z

according to the relation $k_z = \sqrt{\frac{2m(E_k + V_0)}{\hbar^2} - k_{//}^2} + \frac{p_z}{\hbar}$, where m is the free-electron mass, E_k

photoelectron kinetic energy, V_0 the inner potential set to 15 eV, and p_z the photon momentum correction in our experimental geometry [35].

The map in Fig. 2 clearly shows FS contours of the d_{xz} -derived interfacial states whose intensity periodically blows up when k_z hits the Γ -points of the BZ. However, this pattern alone does not necessarily indicate a 3D-ity of these states, because 2D states formed by the out-of-plane d_{xz} -orbitals confined in the interfacial QW would also produce periodic intensity oscillations. The only difference is that the out-of-plane dispersion of the 3D states will manifest itself as rounded FS contours in the (k_x, k_z) coordinates, and the absence of it for the 2D states as straight FS contours (for in-depth analysis of ARPES response of 2D states see [45]). In our case, relatively poor statistics and variations of the photoemission matrix element with $h\nu$ and k_x do not allow reliable discrimination between these 2D and 3D patterns of the k_z -dependent ARPES intensity from the MES. As the acquisition of this dataset has already required more than 5 hrs, further increase of the acquisition time for these off-resonance measurements is less practical.

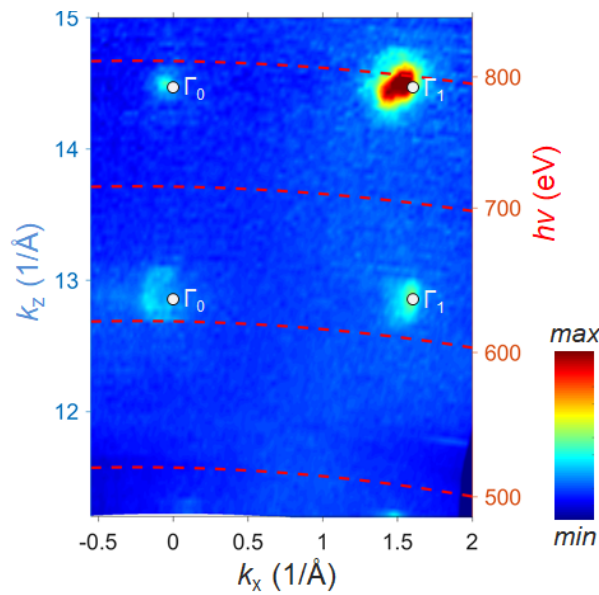


Fig. 2. The d_{xz} -derived FS in PA-LAO/STO as a function of k_z in an extended $h\nu$ -range. The corresponding $h\nu$ -values are marked. The intensity is normalized to the angle-integrated intensity for each $h\nu$. The 3D-ity of the out-of-plane MES states, suggested by rounded FS contours, is confirmed by the k_F variations across the BZs in Fig. 3.

In order to confirm the 3D-ity of the X-ray induced MES, we returned to the resonant $h\nu = 466.4$ eV delivering maximal intensity to the d_{yz} -states, and investigated the variation of the apparent k_F as a function of $\mathbf{k}_{//}$ when moving to the next BZ. The measured ARPES image through two BZs is presented in Fig 4 (a). As in our case the occupied bandwidth $W \sim 50$ meV is basically equal to the experimental ΔE , accurate determination of k_F is not trivial. Our ARPES simulations, described in the Appendix, have demonstrated that whereas the conventional method to determine k_F from the peaks of spectral intensity at E_F (intensity method) stays accurate only as long as W is much larger than ΔE , the extremes of the gradient dI_w/dk of the bandwidth-integrated spectral intensity (gradient method) yield accurate k_F values even when W is of the order of or even smaller than ΔE . The experimental dI_w/dk (in our case integrated over an energy window of 100 meV, with the excluded polaronic introducing a negligible correction) is shown in Fig. 3 (b). Relevant

for our MES dimensionality analysis is the d_{yz} -band, where the dI_W/dk extremes marked k_F^0 and k_F^1 identify its apparent k_F (for the k_F -determination method see Appendix). Remarkably, it reduces from $k_F^0 \sim 0.44 \text{ \AA}^{-1}$ in the first BZ to $k_F^1 \sim 0.29 \text{ \AA}^{-1}$ in the second one (hereinafter the accuracy of all k_F values, including the statistical and instrumental errors, is about $\pm 0.025 \text{ \AA}^{-1}$). We note that on the left side of Γ_0 and right side of Γ_1 the spectral intensity from this band vanishes before reaching E_F , presumably due to a sharp variation of the photoemission matrix elements with \mathbf{k} , and can not be used to determine \mathbf{k}_F . For another PA-LAO/STO sample, where the post-growth annealing time was increased to 24 hrs, we found a somewhat smaller $k_F^0 \sim 0.40 \text{ \AA}^{-1}$ that anyway reduced to $k_F^1 \sim 0.29 \text{ \AA}^{-1}$ in the second BZ. Furthermore, we have compared our results on PA-LAO/STO with previous resonant SX-ARPES measurements on bare STO (Supplementary in Ref. [22]) and have found in this reference system remarkably similar $k_F^0 \sim 0.40 \text{ \AA}^{-1}$ and $k_F^1 \sim 0.29 \text{ \AA}^{-1}$.

This difference of the apparent k_F between the two BZs is actually a clear manifestation of the 3D character of the d_{yz} band in both PA-LAO/STO and STO. This situation is sketched in Fig. 3 (c), showing the d_{yz} -derived FS sheet measured in our experiment. In this case the $k_{//}$ -coordinate of \mathbf{k}_F indeed depends on k_z , which decreases as $k_{//}$ increases into the next BZ. The effect of the relatively small change of k_z between the two BZs on the apparent k_F is amplified by the strong elongation of the FS sheets along the k_x -axis, with light- and heavy-electron axes being ~ 0.12 and 0.8 \AA^{-1} , respectively, as measured in the previous polarization-dependent studies on for PA-LAO/STO [14,22] and STO [17,18]. We note that our $h\nu = 466.4 \text{ eV}$ at the Ti L_2 -edge resonance corresponds to $k_z = 6.99 (2\pi/a)$, i.e. brings k_z almost ideally to the Γ -point of bulk STO where the MES is located. Had the L -edge intra-atomic resonance energy not coincided with the Γ -point, the spectral intensity from the MES would have hugely dropped, and the ARPES data acquisition would have required much longer acquisition time similarly to the dataset presented in Fig. 2.

Our SX-ARPES results on PA-LAO/STO and STO can be compared to the VUV-ARPES results of Plumb *et al.* [44] on STO surfaces prepared by annealing in vacuum. In this case, the emergent MES can be related to the V_{Os} only [14–22], without any intrinsic polar-discontinuity contribution. In line with our findings, the experimental k_z -dispersions measured in an $h\nu$ range below 100 eV have also demonstrated the 2D-ity of the Ti d_{xy} states and 3D-ity of the $d_{xz/yz}$ ones, with the latter forming closed contours in the out-of-plane FS map [44]. An indirect confirmation of the 3D character of the X-ray generated MES is an observation that such MES has a higher mobility compared to the intrinsic one [33] that can be attributed to its extension from the interface into the defect-free STO bulk.

Remarkably, the ST-samples show a qualitatively different pattern of the ARPES variations with $k_{//}$. Fig. 4 (a) represents an ARPES image from the dataset of Ref. [11]. This dataset was acquired at the same experimental conditions as above. Although the spectral intensity of the d_{yz} -bands again strongly varies through the BZs, the corresponding dI_W/dk extremes (b) show constant $k_F \sim 0.33 \text{ \AA}^{-1}$, identifying the 2D-ity of the MES. In passing, we note a significantly larger polaronic renormalization of the d_{yz} -dispersion at the ST-LAO/STO interfaces compared to PA-LAO/STO, where the electron-phonon interaction is screened by the larger MES density. Also the two hot spots of the ARPES intensity, where the d_{xy} band intersects the d_{yz} one, are more pronounced for ST-LAO/STO; the larger smearing of the d_{xy} states in PA-LAO/STO can manifest a larger disorder in its top STO layer due to the random X-ray generated V_{Os} in this region.

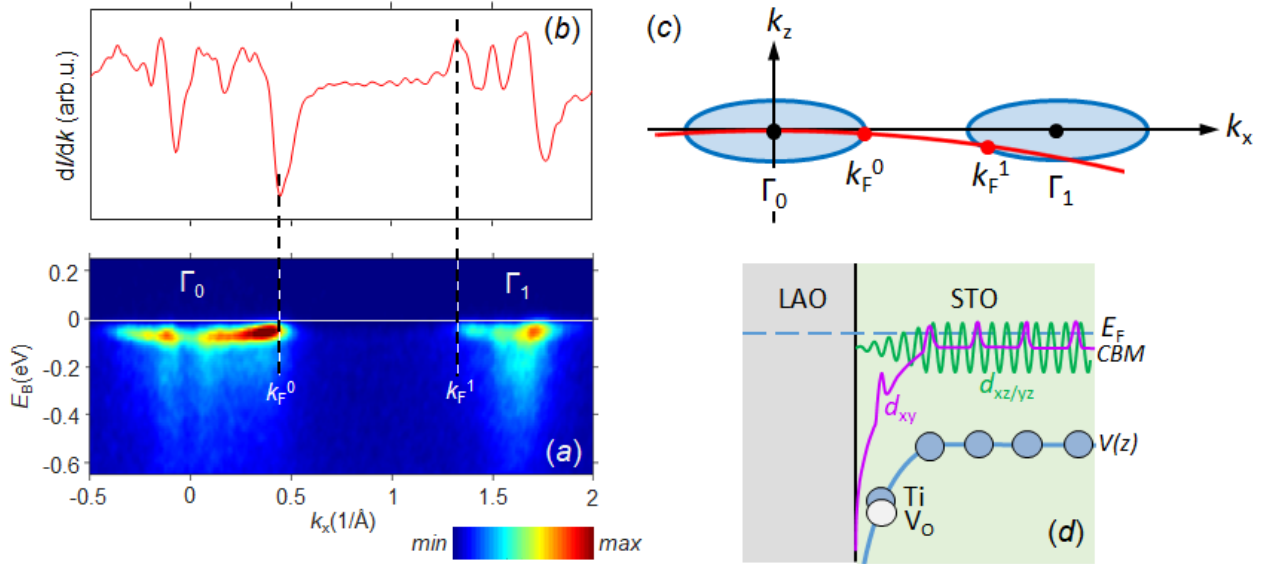


Fig. 3. 3D-MES in PA-LAO/STO: (a) Resonant ARPES image through two BZs measured at $h\nu = 466.4$ eV; (b) corresponding gradient dI_w/dk of the bandwidth-integrated intensity, where the dashed lines mark k_F of the d_{yz} bands. As sketched in (c), the difference in the apparent k_F of the d_{yz} bands between the two BZs identifies the out-of-plane dispersion and thus 3D-MES; (d) Schematics of the sharp interfacial band bending, screened by the additional electrons supplied by the V_O s, and of the corresponding wavefunctions of the d_{xy} and d_{xz} states. The t_{2g} electrons, propagating into the STO bulk, form the 3D-MES.

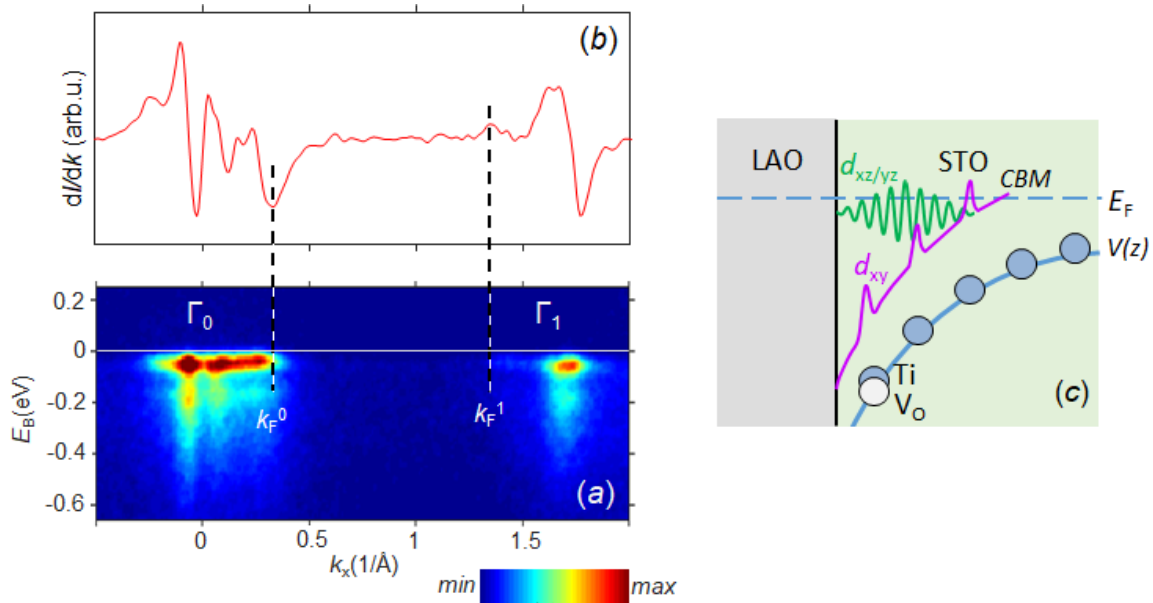


Fig. 4. 2D-MES in ST-LAO/STO: (a) Resonant ARPES image through two BZs measured at $h\nu = 466.4$ eV; (b) dI_w/dk plot, where the dashed lines mark k_F of the d_{yz} bands. Its identical value between the two BZs identify pure 2D-ity of the MES in ST-LAO/STO; (c) Schematics of an interfacial band bending embedding the d_{xy} and quantum-confined $d_{xz/yz}$ states which form the 2D-MES.

We note that recent results by Soltani *et al.* [46] suggest that a 2D-MES may also be realized at bare STO surfaces. This has been identified from a splitting of the $d_{xz/yz}$ -derived states, suggesting their quantum confinement and thus 2D-ity. Obviously, the dimensionality of the MES is determined by the depth and extension of the surface/interfacial QW which, in turn, is sensitive to the stoichiometry and preparation of the samples, which was in-situ cleavage in the experiments by Soltani *et al.* [46] vs in-situ annealing in the experiments by Plumb *et al.* [44]

Discussion

Bulk and interfacial oxygen deficiency in STO

The V_{O_s} , developing under X-ray irradiation, should be one of the key factors of the observed 3D-ity of the MES in PA-LAO/STO, in contrast to the conventional 2D-MES in ST-LAO/STO. First of all, we note that LAO/STO interfaces grown on top of OD-STO have previously been studied by a number of techniques other than ARPES such as magnetotransport [8] and conducting-tip atomic force microscopy of the interfacial cross-section [9]. It has been noted that their n_s can be two-three orders of magnitude larger than $n_s = 0.5$ e per u.c. area predicted by the electrostatic arguments. This fact alone necessitates the existence of an extended and thus 3D component of the MES in OD-samples, and it has indeed been observed that sufficiently high concentrations of V_{O_s} result in a dimensionality transformation of the MES from 2D to 3D [8–10]. Electron mobility in these systems could significantly exceed that of the paradigm 2DES in ST-LAO/STO [8,30,47]; this phenomenon could trace back to stronger electron screening of the polaronic interactions in LAO/STO by larger electron density [11]. However, the V_O distribution profile in these OD-samples would extend into STO by a few thousands of Å and more [48], also affected by oxygen trapping and diffusion at domain walls (see, for example, Refs. [49–51]).

In contrast to these initially-OD samples, the post-annealing of our samples in oxygen, albeit ex-situ, ensures that before the X-ray irradiation they were at most stoichiometric. As discussed above, this fact is evidenced by the initial absence of the IGS peak and Ti^{3+} core-level component in the ARPES spectra. The X-ray generated V_{O_s} should then locate mostly in the top layer of STO because, while easy out-diffusion of oxygen atoms from STO through the LAO overlayer can be explained by typically relaxed crystallinity of the latter [52], the out-diffusion from deeper layers of STO should be practically prohibited due to vanishing diffusion coefficient of oxygen at our low sample temperature. Our case should therefore be different from creation of V_{O_s} by deposition of thin metal films on STO at higher temperature where the V_{O_s} could be distributed over a depth of ~ 1 nm [53,54]. This top-layer location of the V_{O_s} in our case is consistent with the above observation that the Ti^{3+} spectral weight in the TEY-XAS spectra in Fig. 1 (a), which probe a significant depth into STO, is much smaller than in the core-level photoemission spectra in (b), which probe a much narrower vicinity of the interface.

Extended-QW scenario

In view of the 2D-ity of the X-ray generated V_{O_s} , the observed 3D-MES in our PA-LAO/STO samples seems puzzling. Which particular kind of the electron states and $V(z)$ shape is needed to realize such 3D-MES? We will start from the well-known picture of the band bending at the ST-LAO/STO interface [4,6,48] sketched in

Fig. 3 (d). The in-plane d_{xy} orbitals from each TiO_2 plane form a sequence of the d_{xy} electron states localized in the out-of-plane direction, whose energies climb $V(z)$ to cross E_F at a finite distance from the interface. The out-of-plane $d_{xz/yz}$ orbitals from each TiO_2 plane hybridize into electron states delocalized in the out-of-plane direction, which quantize in $V(z)$ to form a ladder of the $d_{xz/yz}$ states (where normally only the lowest one is occupied). With no occupied t_{2g} states propagating into the STO bulk, the MES confined in the interfacial $V(z)$ is purely 2D.

One possibility to realize the 3D behaviour (or rather quasi-3D in this particular context) is to increase the depth extension of $V(z)$, which we will call the *extended-QW scenario*. In this case the 3D states will form as the convergence limit of a ladder of 2D states, quantized in the long-range confining potential, as the extension of this potential increases. Such a 2D- to 3D-dimensionality transformation has previously been demonstrated, for example, for multilayer graphene [55] and anatase TiO_2 [56]. A similar analysis for the bare STO surface [57] has suggested that whereas a confining potential with an extension of a few monolayers can form a 3D-like ladder of QW states out of the d_{xy} states having large perpendicular m^* , it forms only one QW state out of the $d_{xz/yz}$ states with their large interlayer hopping and thus smaller perpendicular m^* . This result for the STO surface, however, is at odds with the experimental k_z dispersions demonstrating that, other way around, the d_{xy} states are 2D [18,44] and the $d_{xz/yz}$ ones are 3D [44]. These experimental results go in line with our observations of the 3D-ity of the $d_{xz/yz}$ states in PA-LAO/STO.

Another way to reconcile the extended-QW scenario with our experimental results might be if the MES contribution injected by the top-layer V_{0s} is significantly more delocalized than the intrinsic polar-discontinuity contribution. To check this scenario, we have performed supercell DFT+SIC electronic structure calculations where a 400-atom supercell incorporating 16 TiO_2 layers, 6 LaO layers and a (2×2) interlayer resolution in a superlattice geometry was employed. As shown in Fig. 5 (a), the oxygen deficiency was simulated with a V_o placed in the top TiO_2 layer. Fig. 5 (b) presents the results of this calculation (red line) in comparison with the stoichiometric interface (blue). We observe that although the V_o somewhat enhances the asymptotics of the MES towards the STO bulk, it essentially does not change its overall depth extension of ~ 2 u.c. compared to ST-LAO/STO, where our ARPES experiment has found a purely 2D intrinsic MES.

Bulk-metallicity scenario

Another possibility to realize 3D-MES would be that under X-ray irradiation the whole STO depth within the light absorption depth becomes metallic, and the depth extension of $V(z)$, other way around, shrinks to enable the ARPES experiment directly access the bulk electronic structure. This *bulk-metallicity* scenario is sketched in Fig. 3 (d). In our case such short-range $V(z)$ seems more relevant than the long-range one in the previous scenario, because the top-layer V_{0s} release additional MES electrons, as manifested by the observed increase of both k_F and lateral conducting fraction [14] under X-ray irradiation. The increased electron density will then more effectively screen the interfacial-potential discontinuity, reducing the depth over which $V(z)$ saturates to below the probing depth in our ARPES experiment. If upon further progression into the STO bulk the CBM stays below E_F , the flat $V(z)$ potential in this region forms the 3D-MES. This scenario explains the 3D-ity of the $d_{xz/yz}$ states observed by the ARPES experiment in PA-LAO/STO. Due to the

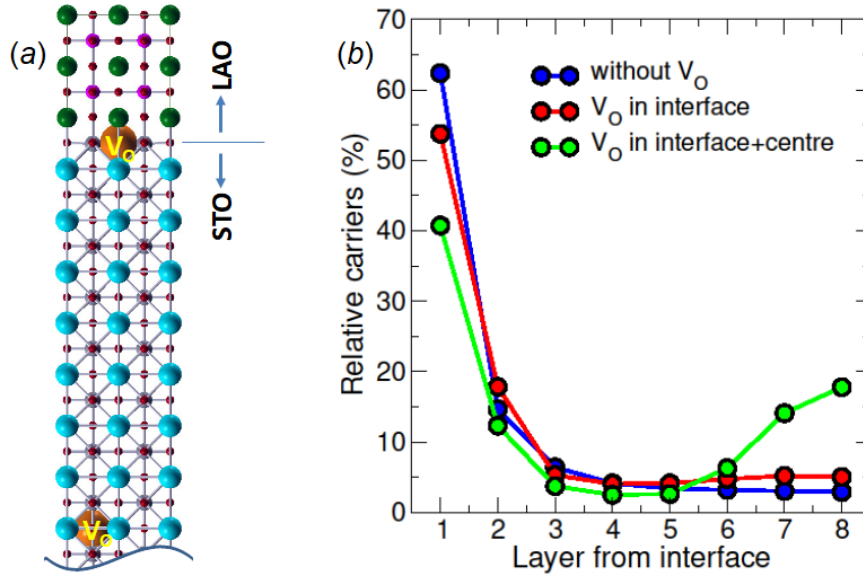


Fig. 5. DFT+SIC calculations: (a) The supercell incorporating V_O s in the top and bulk TiO_2 layers; (b) Calculated layer-resolved MES density for the stoichiometric and OD-LAO/STO interfaces. Note that only the Ti t_{2g} contribution enters here, since this is the major contribution to the MES.

flat potential, in the STO bulk the d_{xy} states degenerate with the $d_{xz/yz}$. Importantly, the bulk metallicity in STO required for such a scenario can only be realized if the X-ray irradiation causes some effective doping throughout the STO bulk. As we discuss below, such metallicity is essentially the well-known (albeit poorly understood) photoconductivity observed in STO-based systems. The scenario of short-range $V(z)$ combined with the bulk metallicity naturally extends from PA-LAO/STO to bare STO surfaces; the 3D-MES in that case can not be explained only by the V_O s [19,20] or any atomic rearrangements [44] in the top STO layer.

One possibility for the bulk metallicity of PA-LAO/STO might be that already before the X-ray irradiation the deeper STO layers contained a minute amount of V_O s below the sensitivity limit of our ARPES and XAS experiments. Fig. 5 (b, green line) shows our calculations which included, in addition to the V_O in the top STO layer, another V_O in the STO-slab centre between the eighth and ninth TiO_2 layer, representing the STO bulk. These results indicate that the extension of the MES induced by the bulk V_O s is similar to the interfacial ones, restricted within a sphere with a radius of ~ 2 u.c. The corresponding wavefunctions will start to overlap, forming the 3D character of the MES, at a concentration of only 1.5% which is below the detection limit of our experiment. The previous DFT calculations by Li et al. [10] showed a roughly twice larger spatial extension of the V_O -induced MES, with the difference to our calculations plausibly attributed to the neglect of electron correlations. Transport measurements [24] indicate a yet smaller V_O -concentration of 0.03% which is necessary to transform STO into 3D metal. Such a minute amount of V_O s could likely stay in our samples after their post-annealing. With STO substrates being typically slightly oxygen-deficient, the same mechanism could be at play to form the 3D-MES at bare STO surfaces. We note that the above picture of the photoinduced DX-centers as electron donors forming an extended MES is actually similar to the conventional semiconductors, where tiny dopant concentrations on the promille level can form delocalized electron gas. The exhaustive picture of the OD-LAO/STO interfaces, including the entangled phenomena of

the interfacial electrostatic field, V_{Os} , intrinsic and V_O -induced MES and photoconductivity, still awaits accurate theoretical description.

The bulk metallicity in STO suggested by this scenario goes in line with the well-known giant photoconductivity of STO-based systems (see, for example, Refs. [32,58][add: Persistent Photoconductivity in 2D electron gases at different oxide interfaces]) that may exceed that in semiconductors by few orders of magnitude [59]. This phenomenon strongly depends on the sample preparation, with the defects including the V_{Os} as well as the cubic-tetragonal phase transition [32] and lattice relaxation [34] playing the main role, and for some LAO/STO [34,60] and OD-STO [59] samples can even become persistent on a time scale of up to days and more. In our experimental setup, we observed the photoconductivity as a drain current to the sample holder through the whole 0.25-mm thickness of our nominally insulating STO substrates which switched on and off under X-ray irradiation. Although the exact physics of photoconductivity in STO yet remains elusive, it is often associated with DX-centers (donor defect) located ~ 200 meV below the conduction-band minimum. This energy position would allow the photoinduced (in our case X-ray induced) electron states to effectively hybridize with the MES wavefunctions, providing coupling between the MES puddles and thus the 3D-ity of the whole system.

Although the above mechanisms explain the emergence of the 3D electron states, the concentration of V_{Os} and the density-of-states of the corresponding MES in the deeper STO layers stays negligible compared to the V_{Os} and associated states generated by X-rays in the interfacial region. Therefore, these mechanisms can not directly explain the whole large density of the X-ray generated 3D-MES. One possible explanation might be that X-rays generate V_{Os} in STO bulk through creation of Frenkel pairs, where the O atom would become interstitial without the necessity to diffuse over a large distance. This behavior may be facilitated by the repulsion of the X-ray generated mobile electrons from the ones localized at the V_{Os} [34]. Furthermore, the Frenkel-pair mechanism would be consistent with the fact pointed out above that an increase of temperature above ~ 100 K quenches the spectroscopic signatures of the V_{Os} . However, we could not computationally confirm or rule out this scenario within any reasonable computational effort. Full understanding of the X-ray induced formation of the 3D-MES in LAO/STO requires therefore further experimental and theoretical investigations.

Summary

We used soft-X-ray ARPES to investigate electronic structure of LAO/STO samples grown at low oxygen pressure and post-annealed ex-situ till their (nearly) complete stoichiometric recovery. Under X-ray irradiation at low temperatures below ~ 100 K, the ARPES spectra of these samples show a rapid development of the Ti^{3+} component of the Ti $2p$ core levels and IGS peak, characteristic of the V_{Os} , in parallel with scaling up of the MES spectral weight. Given that at this temperature the oxygen out-diffusion is suppressed, these V_{Os} should be located mostly in the top STO layer. However, the out-of-plane electron dispersions evaluated from the off-resonant ARPES data as well as the variation of the k_{\parallel} values over the BZs, evaluated by the gradient method from the Ti $2p$ resonant data, evidence that the X-ray generated MES in our PA-LAO/STO samples is 3D, extending deep into the STO bulk. This behavior, essentially identical to the X-ray generated MES in STO, is clearly distinct from the intrinsic MES in ST-LAO/STO samples, fairly immune to X-ray irradiation, where our ARPES experiment finds pure 2D-ity of the MES. Our DFT+SIC

calculations indicate that the spatial extension of the MES induced by V_{0s} in the STO bulk as well as in the top STO layer is about 2 u.c. which can hardly explain the 3D-ty of the MES in PA-LAO/STO. One scenario of this phenomenon, the extended-QW one, involves formation of a dense ladder of QW states in a long-range interfacial potential. More likely in our case is however the bulk-metallicity scenario of the observed 3D-ty, where the X-ray-induced bulk metallicity in STO is accompanied by a short-range interfacial $V(z)$ allowing the ARPES experiment to directly access the bulk states. In this case the formation of the 3D-MES may involve the minute concentrations of V_{0s} remnant in the STO bulk and the well-known photoconductivity of STO, and even more exotic mechanisms such as X-ray induced formation of Frenkel pairs. The short-range character of $V(z)$ can be caused by a large concentration of the X-ray generated V_{0s} and thus MES density in the top STO layer, where it effectively screens the interfacial $V(z)$ discontinuity.

Acknowledgments

We thank C. Cancellieri, R. de Souza and G. Drera for sharing fruitful discussions, and M. Radovic for giving us access to the PLD facility. A.C. acknowledges funding from the Swiss National Science Foundation under grant no. 200021_165529, and F.A. under grant no. 200020B_188709. M.-A.H. acknowledges the support by the Swiss Excellence Scholarship grant ESKAS-no. 2015.0257 and the Romanian UEFISCDI Agency under Contracts No. 475 PN-III-P4-ID-PCE-2020-2540.

Appendix: Gradient vs intensity method of the k_F determination

A crucial element of our further analysis of the ARPES data is accurate determination of the MES' k_F . In fact, its signatures in the ARPES intensity can be strongly distorted not only by sharp variations of the photoemission matrix element but also by broadening of the experimental spectra due incoherent electron scattering (including defects) and limited experimental resolution in \mathbf{k} and E_b . Conventionally, one determines from the maxima of the momentum-distribution curve of the spectral intensity at E_F (Fermi intensity I_F). However, Straub *et al* [60] have shown that the applicability of this so-called intensity method is restricted to wide-band systems, where the occupied quasiparticle bandwidth W much exceeds ΔE the experimental resolution, and that in the general case, including narrow-band systems, extremes of the gradient dI_w/dk of the spectral intensity integrated through the whole W resolve k_F with much higher accuracy. In fact, this so-called gradient method is based on the theoretical many-body definition of the Fermi surface (FS) as restricted by the extremal gradients of the momentum distribution function $n(\mathbf{k})$ [60].

To identify the optimal k_F -determination method in our case, we performed ARPES simulations for a 2D (or 2D cross-section of 3D) parabolic band whose parameters $W = 50$ meV and $k_F = 0.4 \text{ \AA}^{-1}$ closely resembled the d_{yz} band along k_x . With the electron lifetime broadening being negligible close to E_F , the corresponding spectral function $A(E, \mathbf{k})$ was modelled as the δ -function centered at the band's dispersion $E(\mathbf{k})$ and terminated at E_F . Its ARPES response was simulated by Gaussian convolution with FWHM = 50 meV in the E -direction describing the experimental ΔE , and 0.1 \AA^{-1} in the \mathbf{k} -direction describing the combined effect of disorder and experimental \mathbf{k} -resolution.

The results of these simulations, corresponding to the case $W = \Delta E$, are presented in Fig. A1 (b) as the ARPES intensity with the corresponding $I_F(k)$ and dI_w/dk curves on top. Whereas the intensity method to

determine k_F from the peaks of I_F underestimates its value as much as 14%, the extremes of the gradient dI_W/dk yield its value with a remarkable precision of $\sim 0.25\%$. Important for the gradient-method accuracy is that the spectral intensity is integrated over the whole bandwidth, because the gradient dI_F/dk of the Fermi intensity only, also shown in Fig. A1 (b), overestimates the actual k_F by 2.5%. Therefore, our ARPES simulations clearly demonstrate that the gradient method to determine k_F is optimal in our case.

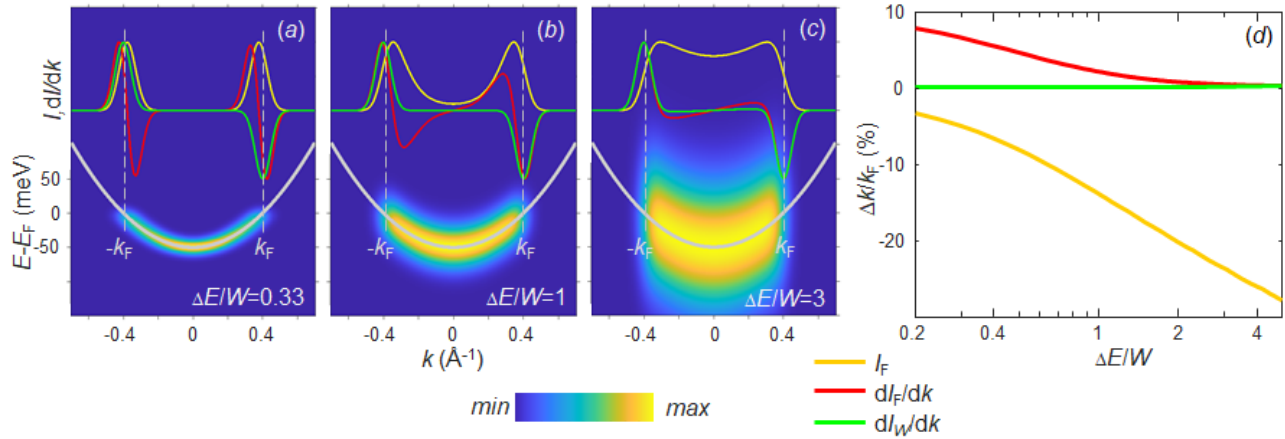


Fig. A1. Determination of k_F at different experimental ΔE vs the occupied bandwidth W : (a-c) Band dispersion superimposed with the ARPES intensity (*bottom*) and the corresponding characteristics of k_F - $I_F(k)$, bandwidth-integrated dI_W/dk , and dI_F/dk - for different $\Delta E/W$ values; (d) Deviation of the peaks in these curves from the true k_F as a function of $\Delta E/W$. The dI_W/dk peaks deliver the most accurate k_F value through all $\Delta E/W$ values.

Our ARPES simulations extended to smaller and larger $\Delta E/W$ values are shown in Fig. A1 (a) and (c), respectively. Obviously, the intensity method improves its accuracy towards small ΔE , whereas the I_F gradient does so towards large ΔE compared to W . This trend calculated over a wide range of $\Delta E/W$ is presented in the panel (d) which shows the relative deviation of the $I_F(k)$, dI_W/dk and dI_F/dk extremes from the true k_F . A reduction of the spectral k -broadening will increase the accuracy of the intensity and I_F -gradient methods, in particular of the latter. However, the dI_W/dk gradient method stays remarkably accurate through the whole range of ΔE compared to W , with a negligible rms deviation of only 0.3% even with the relatively large k -broadening used in our simulations. The gradient method to determine k_F can therefore be deemed the most universal. An added advantage of this method is that the narrower width of the dI_W/dk peaks compared to $I_F(k)$ makes it less susceptible to the photoemission matrix-element variations with k .

References

- [1] Tokura Y 2000 Orbital Physics in Transition-Metal Oxides *Science* **288** 462–8
- [2] Mannhart J and Schlom D G 2010 Oxide Interfaces--An Opportunity for Electronics *Science* **327** 1607–11
- [3] Hwang H Y, Iwasa Y, Kawasaki M, Keimer B, Nagaosa N and Tokura Y 2012 Emergent phenomena at oxide interfaces *Nature Materials* **11** 103–13

- [4] Delugas P, Filippetti A, Fiorentini V, Bilc D I, Fontaine D and Ghosez P 2011 Spontaneous 2-Dimensional Carrier Confinement at the n-Type SrTiO₃/LaAlO₃ Interface *Physical Review Letters* **106** 166807
- [5] King P D C, McKeown Walker S, Tamai A, de la Torre A, Eknapakul T, Buaphet P, Mo S-K, Meevasana W, Bahramy M S and Baumberger F 2014 Quasiparticle dynamics and spin-orbital texture of the SrTiO₃ two-dimensional electron gas *Nature Communications* **5** 3414
- [6] Cancellieri C, Reinle-Schmitt M L, Kobayashi M, Strocov V N, Willmott P R, Fontaine D, Ghosez P, Filippetti A, Delugas P and Fiorentini V 2014 Doping-dependent band structure of LaAlO₃/SrTiO₃ interfaces by soft x-ray polarization-controlled resonant angle-resolved photoemission *Physical Review B* **89** 121412(R)
- [7] Caputo M, Boselli M, Filippetti A, Lemal S, Li D, Chikina A, Cancellieri C, Schmitt T, Triscone J-M, Ghosez P, Gariglio S and Strocov V N 2020 Artificial quantum confinement in LaAlO₃/SrTiO₃ heterostructures *Physical Review Materials* **4** 035001
- [8] Herranz G, Basletić M, Bibes M, Carrétéro C, Tafra E, Jacquet E, Bouzehouane K, Deranlot C, Hamzić A, Broto J-M, Barthélémy A and Fert A 2007 High Mobility in LaAlO₃/SrTiO₃ Heterostructures: Origin, Dimensionality, and Perspectives *Physical Review Letters* **98** 216803
- [9] Basletic M, Maurice J-L, Carrétéro C, Herranz G, Copie O, Bibes M, Jacquet É, Bouzehouane K, Fusil S and Barthélémy A 2008 Mapping the spatial distribution of charge carriers in LaAlO₃/SrTiO₃ heterostructures *Nature Materials* **7** 621–5
- [10] Li Y, Phattalung S N, Limpijumnong S, Kim J and Yu J 2011 Formation of oxygen vacancies and charge carriers induced in the n-type interface of a LaAlO₃ overlayer on SrTiO₃(001) *Physical Review B* **84** 245307
- [11] Cancellieri C, Mishchenko A S, Aschauer U, Filippetti A, Faber C, Barišić O S, Rogalev V A, Schmitt T, Nagaosa N and Strocov V N 2016 Polaronic metal state at the LaAlO₃/SrTiO₃ interface *Nature Communications* **7** 10386
- [12] Strocov V N, Cancellieri C and Mishchenko A S 2018 Electrons and Polarons at Oxide Interfaces Explored by Soft-X-Ray ARPES *Spectroscopy of Complex Oxide Interfaces* 107–51
- [13] Scopigno N, Bucheli D, Caprara S, Biscaras J, Bergeal N, Lesueur J and Grilli M 2016 Phase Separation from Electron Confinement at Oxide Interfaces *Physical Review Letters* **116** 026804
- [14] Strocov V N, Chikina A, Caputo M, Husanu M-A, Bisti F, Bracher D, Schmitt T, Miletto Granozio F, Vaz C A F and Lechermann F 2019 Electronic phase separation at LaAlO₃/SrTiO₃ interfaces tunable by oxygen deficiency *Physical Review Materials* **3** 106001
- [15] Santander-Syro A F, Copie O, Kondo T, Fortuna F, Pailhès S, Weht R, Qiu X G, Bertran F, Nicolaou A, Taleb-Ibrahimi A, Le Fèvre P, Herranz G, Bibes M, Reyren N, Apertet Y, Lecoœur P, Barthélémy A and Rozenberg M J 2011 Two-dimensional electron gas with universal subbands at the surface of SrTiO₃

- [16] Meevasana W, King P D C, He R H, Mo S-K, Hashimoto M, Tamai A, Songsirittigul P, Baumberger F and Shen Z-X 2011 Creation and control of a two-dimensional electron liquid at the bare SrTiO₃ surface *Nature Materials* **10** 114–8
- [17] Walker S M, Bruno F Y, Wang Z, de la Torre A, Riccò S, Tamai A, Kim T K, Hoesch M, Shi M, Bahramy M S, King P D C and Baumberger F 2015 Carrier-Density Control of the SrTiO₃(001) Surface 2D Electron Gas studied by ARPES *Advanced Materials* **27** 3894–9
- [18] Wang Z, McKeown Walker S, Tamai A, Wang Y, Ristic Z, Bruno F Y, de la Torre A, Riccò S, Plumb N C, Shi M, Hlawenka P, Sánchez-Barriga J, Varykhalov A, Kim T K, Hoesch M, King P D C, Meevasana W, Diebold U, Mesot J, Moritz B, Devereaux T P, Radovic M and Baumberger F 2016 Tailoring the nature and strength of electron–phonon interactions in the SrTiO₃(001) 2D electron liquid *Nature Materials* **15** 835–9
- [19] Dudy L, Sing M, Scheiderer P, Denlinger J D, Schütz P, Gabel J, Buchwald M, Schlueter C, Lee T-L and Claessen R 2016 In Situ Control of Separate Electronic Phases on SrTiO₃ Surfaces by Oxygen Dosing *Advanced Materials* **28** 7443–9
- [20] Gabel J, Zapf M, Scheiderer P, Schütz P, Dudy L, Stübinger M, Schlueter C, Lee T-L, Sing M and Claessen R 2017 Disentangling specific versus generic doping mechanisms in oxide heterointerfaces *Physical Review B* **95** 195109
- [21] Sing M, Jeschke H O, Lechermann F, Valentí R and Claessen R 2017 Influence of oxygen vacancies on two-dimensional electron systems at SrTiO₃-based interfaces and surfaces *The European Physical Journal Special Topics* **226** 2457–75
- [22] Chikina A, Lechermann F, Husanu M-A, Caputo M, Cancellieri C, Wang X, Schmitt T, Radovic M and Strocov V N 2018 Orbital Ordering of the Mobile and Localized Electrons at Oxygen-Deficient LaAlO₃/SrTiO₃ Interfaces *ACS Nano* **12** 7927–35
- [23] Jeschke H O, Shen J and Valentí R 2015 Localized versus itinerant states created by multiple oxygen vacancies in SrTiO₃ *New Journal of Physics* **17** 023034
- [24] Frederikse H P R, Thurber W R and Hosler W R 1964 Electronic Transport in Strontium Titanate *Physical Review* **134** A442–5
- [25] Pavlenko N, Kopp T, Tsymbal E Y, Sawatzky G A and Mannhart J 2012 Magnetic and superconducting phases at the LaAlO₃/SrTiO₃ interface: The role of interfacial Ti 3d electrons *Physical Review B* **85** 020407(R)
- [26] Lin C and Demkov A A 2013 Electron Correlation in Oxygen Vacancy in SrTiO₃ *Physical Review Letters* **111** 217601
- [27] Lechermann F, Boehnke L, Grieger D and Piefke C 2014 Electron correlation and magnetism at the

LaAlO₃/SrTiO₃ interface: A DFT DMFT investigation *Physical Review B* **90** 085125

- [28] Lechermann F, Jeschke H O, Kim A J, Backes S and Valentí R 2016 Electron dichotomy on the SrTiO₃ defect surface augmented by many-body effects *Physical Review B* **93**
- [29] Altmeyer M, Jeschke H O, Hijano-Cubelos O, Martins C, Lechermann F, Koepernik K, Santander-Syro A F, Rozenberg M J, Valentí R and Gabay M 2016 Magnetism, Spin Texture, and In-Gap States: Atomic Specialization at the Surface of Oxygen-Deficient SrTiO₃ *Physical Review Letters* **116** 157203
- [30] Cancellieri C, Reyren N, Gariglio S, Caviglia A D, Fête A and Triscone J-M 2010 Influence of the growth conditions on the LaAlO₃/SrTiO₃ interface electronic properties *EPL (Europhysics Letters)* **91** 17004
- [31] Wang F F Y and Gupta K P 1973 Phase transformation in the oxides *Metallurgical Transactions* **4** 2767–79
- [32] Zhang H, Yan L and Habermeier H-U 2013 Unusual ultraviolet photoconductivity in single crystalline SrTiO₃ *Journal of Physics: Condensed Matter* **25** 035802
- [33] Guduru V K, del Aguila A G, Wenderich S, Kruize M K, McCollam A, Christianen P C M, Zeitler U, Brinkman A, Rijnders G, Hilgenkamp H and Maan J C 2013 Optically excited multi-band conduction in LaAlO₃/SrTiO₃ heterostructures *Applied Physics Letters* **102** 051604
- [34] Tebano A, Fabbri E, Pergolesi D, Balestrino G and Traversa E 2012 Room-Temperature Giant Persistent Photoconductivity in SrTiO₃/LaAlO₃ Heterostructures *ACS Nano* **6** 1278–83
- [35] Strocov V N, Wang X, Shi M, Kobayashi M, Krempasky J, Hess C, Schmitt T and Patthey L 2014 Soft-X-ray ARPES facility at the ADDRESS beamline of the SLS: concepts, technical realisation and scientific applications *Journal of Synchrotron Radiation* **21** 32–44
- [36] Strocov V N, Schmitt T, Flechsig U, Schmidt T, Imhof A, Chen Q, Raabe J, Betemps R, Zimoch D, Krempasky J, Wang X, Grioni M, Piazzalunga A and Patthey L 2010 High-resolution soft X-ray beamline ADDRESS at the Swiss Light Source for resonant inelastic X-ray scattering and angle-resolved photoelectron spectroscopies *Journal of Synchrotron Radiation* **17** 631–43
- [37] Braun J, Minár J, Mankovsky S, Strocov V N, Brookes N B, Plucinski L, Schneider C M, Fadley C S and Ebert H 2013 Exploring the XPS limit in soft and hard x-ray angle-resolved photoemission using a temperature-dependent one-step theory *Physical Review B* **88** 205409
- [38] Körner W and Elsässer C 2010 First-principles density functional study of dopant elements at grain boundaries in ZnO *Physical Review B* **81** 085324
- [39] Drera G, Banfi F, Federici Canova F, Borghetti P, Sangaletti L, Bondino F, Magnano E, Huijben J, Huijben M, Rijnders G, Blank D H A, Hilgenkamp H and Brinkman A 2011 Spectroscopic evidence of in-gap states at the SrTiO₃/LaAlO₃ ultrathin interfaces *Applied Physics Letters* **98** 052907
- [40] Koitzsch A, Ocker J, Knupfer M, Dekker M C, Dörr K, Büchner B and Hoffmann P 2011 In-gap electronic

structure of LaAlO₃-SrTiO₃ heterointerfaces investigated by soft x-ray spectroscopy *Physical Review B* **84** 245121

- [41] Berner G, Sing M, Fujiwara H, Yasui A, Saitoh Y, Yamasaki A, Nishitani Y, Sekiyama A, Pavlenko N, Kopp T, Richter C, Mannhart J, Suga S and Claessen R 2013 Directk-Space Mapping of the Electronic Structure in an Oxide-Oxide Interface *Physical Review Letters* **110** 247601
- [42] Cancellieri C, Reinle-Schmitt M L, Kobayashi M, Strocov V N, Schmitt T, Willmott P R, Gariglio S and Triscone J-M 2013 Interface Fermi States of LaAlO₃/SrTiO₃ and Related Heterostructures *Physical Review Letters* **110** 137601
- [43] Drera G, Salvinelli G, Bondino F, Magnano E, Huijben M, Brinkman A and Sangaletti L 2014 Intrinsic origin of interface states and band-offset profiling of nanostructured LaAlO₃/SrTiO₃ heterojunctions probed by element-specific resonant spectroscopies *Physical Review B* **90** 035124
- [44] Plumb N C, Salluzzo M, Razzoli E, Månsson M, Falub M, Krempasky J, Matt C E, Chang J, Schulte M, Braun J, Ebert H, Minár J, Delley B, Zhou K-J, Schmitt T, Shi M, Mesot J, Patthey L and Radović M 2014 Mixed Dimensionality of Confined Conducting Electrons in the Surface Region of SrTiO₃ *Physical Review Letters* **113** 086801
- [45] Strocov V N 2018 Photoemission response of 2D electron states *Journal of Electron Spectroscopy and Related Phenomena* **229** 100–7
- [46] Soltani S, Cho S, Ryu H, Han G, Kim B, Song D, Kim T K, Hoesch M and Kim C 2017 dxz/yz orbital subband structures and chiral orbital angular momentum in the (001) surface states of SrTiO₃ *Physical Review B* **95** 125103
- [47] Kalabukhov A, Gunnarsson R, Börjesson J, Olsson E, Claeson T and Winkler D 2007 Effect of oxygen vacancies in theSrTiO₃substrate on the electrical properties of theLaAlO₃/SrTiO₃interface *Physical Review B* **75** 121404
- [48] Gariglio S, Fête A and Triscone J-M 2015 Electron confinement at the LaAlO₃/SrTiO₃ interface *Journal of Physics: Condensed Matter* **27** 283201
- [49] Kalisky B, Spanton E M, Noad H, Kirtley J R, Nowack K C, Bell C, Sato H K, Hosoda M, Xie Y, Hikita Y, Woltmann C, Pfanzelt G, Jany R, Richter C, Hwang H Y, Mannhart J and Moler K A 2013 Locally enhanced conductivity due to the tetragonal domain structure in LaAlO₃/SrTiO₃ heterointerfaces *Nature Materials* **12** 1091–5
- [50] Kim Y, Disa A S, Babakol T E, Fang X and Brock J D 2015 Strain and oxygen vacancy ordering inSrTiO₃: Diffuse x-ray scattering studies *Physical Review B* **92** 064105
- [51] Yazdi-Rizi M, Marsik P, Mallett B P P and Bernhard C 2017 Anisotropy of infrared-active phonon modes in the monodomain state of tetragonal SrTiO₃ (110) *Physical Review B* **95** 195107
- [52] Warusawithana M P, Richter C, Mundy J A, Roy P, Ludwig J, Paetel S, Heeg T, Pawlicki A A, Kourkoutis L F,

Zheng M, Lee M, Mulcahy B, Zander W, Zhu Y, Schubert J, Eckstein J N, Muller D A, Stephen Hellberg C, Mannhart J and Schlom D G 2013 LaAlO₃ stoichiometry is key to electron liquid formation at LaAlO₃/SrTiO₃ interfaces *Nature Communications* **4** 2351

- [53] Rödel T C, Fortuna F, Sengupta S, Frantzeskakis E, Le Fèvre P, Bertran F, Mercey B, Matzen S, Agnus G, Maroutian T, Lecoer P and Santander-Syro A F 2016 Universal Fabrication of 2D Electron Systems in Functional Oxides *Advanced Materials* **28** 1976–80
- [54] Kormondy K J, Gao L, Li X, Lu S, Posadas A B, Shen S, Tsoi M, McCartney M R, Smith D J, Zhou J, Lev L L, Husanu M-A, Strocov V N and Demkov A A 2018 Large positive linear magnetoresistance in the two-dimensional t_{2g} electron gas at the EuO/SrTiO₃ interface *Scientific Reports* **8** 7721
- [55] Ohta T, Bostwick A, McChesney J L, Seyller T, Horn K and Rotenberg E 2007 Interlayer Interaction and Electronic Screening in Multilayer Graphene Investigated with Angle-Resolved Photoemission Spectroscopy *Physical Review Letters* **98** 206802
- [56] Moser S, Jovic V, Koch R, Moreschini L, Oh J-S, Jozwiak C, Bostwick A and Rotenberg E 2018 How to extract the surface potential profile from the ARPES signature of a 2DEG *Journal of Electron Spectroscopy and Related Phenomena* **225** 16–22
- [57] Santander-Syro A F, Dai J, Rödel T C, Frantzeskakis E, Fortuna F, Weht R and Rozenberg M J 2020 Quantum interference effects of out-of-plane confinement on two-dimensional electron systems in oxides *Physical Review B* **102** 075101
- [58] Chen Y, Lechaux Y, Casals B, Guillet B, Minj A, Gázquez J, Méchin L and Herranz G 2020 Photoinduced Persistent Electron Accumulation and Depletion in LaAlO₃/SrTiO₃ Quantum Wells *Physical Review Letters* **124** 246804
- [59] Poole V M, Jokela S J and McCluskey M D 2017 Using persistent photoconductivity to write a low-resistance path in SrTiO₃ *Scientific Reports* **7** 6659
- [60] Straub T, Claessen R, Steiner P, Hüfner S, Eyert V, Friemelt K and Bucher E 1997 Many-body definition of a Fermi surface: Application to angle-resolved photoemission *Physical Review B* **55** 13473–8